09

Broadband EPR-spectroscopy and crystal field of Ho³⁺ centers in YAIO₃

© G.R. Asatryan^{1,4}, G.S. Shakurov², B.Z. Malkin³, A.V. Batueva¹, A.G. Petrosyan⁴

¹ loffe Institute,

St. Petersburg, Russia

² Zavoisky Physical-Technical Institute, FRC Kazan Scientific Center of RAS,

Kazan, Russia

³ Kazan Federal University,

Kazan, Tatarstan, Russia

⁴ Institute for Physical Research, National Academy of Sciences of Armenia,

Ashtarak-2, Armenia

E-mail: hike.asatryan@mail.ioffe.ru

Received May 27, 2025 Revised June 19, 2025 Accepted June 25, 2025

YAlO₃:Ho (1.5 at.%) crystals were studied by the method of tunable broadband EPR spectroscopy in sub-THz-band. EPR spectra of holmium ions with the resolved hyperfine structure correspond to resonant transitions between electron-nuclear sublevels of the ground and first excited singlets of the main multiplet 5I_8 of Ho^{3+} ions substituting Y^{3+} ions in two magnetically inequivalent positions, the multiplet being split in crystal field of C_s symmetry. In addition, EPR spectra of $Ho^{3+}-Ho^{3+}$ dimers are also registered, which contain the nearest holmium ions in the magnetically equivalent positions. Crystal field parameters were obtained within the framework of the exchange charge model, and calculations of Stark splittings, constants of hyperfine structure, g-factors of isolated center and dimer were performed. These calculations are compared with optical spectroscopy data reported in the literature and with the experimental results of this study. The validity of the theoretical model was verified by calculating the characteristics of the previously studied crystal YAlO₃:Tm.

Keywords: electron paramagnetic resonance, yttrium orthoaluminate, rare earth elements, dimers.

DOI: 10.61011/PSS.2025.06.61697.145-25

1. Introduction

Yttrium orthoaluminate crystals YAlO₃ (YAP) with orthorhombic structure, together with yttrium-aluminum garnet Y₃Al₅O₁₂ (YAG), activated with Ho³⁺ ions are widely used to excite laser generation in a wide spectral range from blue to three-micron [1-4]. Laser radiation in the two-micron area on the transition of ${}^5I_8 \rightarrow {}^5I_7$ Ho³⁺ ions that corresponds to the window of absolute transparency of atmosphere and is safe for human eyes, is of special interest. YAP: Ho crystals combine good spectroscopic, thermal and mechanical properties. Thanks to natural birefringence, absorption and emission depend on polarization, i.e. on crystal orientation. Contrary to Y₃Al₅O₁₂ with cubic structure, YAlO₃ has orthorhombic symmetry and a closer packing. Ho³⁺ ions enter the lattice in positions of Y^{3+} ions with point symmetry C_s in the environment of 8 closest oxygen atoms and the ninth atom of oxygen at a somewhat longer distance [5] and create two crystallographically equivalent, but magnetically inequivalent paramagnetic centers, Ho1 and Ho2. YAP: Ho crystals are promising for use in optical communications, radar location, remote sensing of atmosphere, mechanical treatment of materials and medicine.

Spectroscopic properties of crystals with $\mathrm{Ho^{3+}}$ ions were studied using the method of electron paramagnetic resonance (EPR) in a number of crystals, including

 KY_3F_{10} : Ho [6], Mg_2SO_4 [7], $CaWO_4$: Ho [8]. In our previous papers [9,10] Ho^{3+} ions in YAG: Ho crystals, which substitute for Y^{3+} ions in dodecahedral lattice sites, were detected and studied using the method of broadband EPR spectroscopy. The values of g-factor (16.4), the hyperfine structure constant (10.88 GHz) and energy interval between the ground and first excited sublevels of the main multiplet 5I_8 of Ho^{3+} ion (119.81 GHz) were determined [9]. In [10], Ho^{3+} ions with an antisite defect, as well as a trigonal Ho^{3+} substituting AI^{3+} in octahedral lattice sites were studied; the spectroscopic parameters of the latter were determined which differ significantly from those of Ho^{3+} localized in dodecahedral sites.

The purpose of this article is a study of EPR of Ho³⁺ ions in a crystal of yttrium orthoaluminate and modeling of the spectra in low-symmetry crystal fields, which act on holmium ions in the crystal lattice. We used our experimental data obtained from broadband EPR — spectroscopy for Ho³⁺ and Tm³⁺ ions [11], as well as literature data of optical measurements.

2. Crystal growth and experiment

YAP single crystals activated with Ho³⁺ ions were grown by the Bridgman method in the Institute for Physical Research of the National Academy of Sciences of the Republic of Armenia (Ashtarak). Modification of the Bridgman method in respect to the growth of high-melting oxides (Al₂O₃, YAG etc.) was developed in 1960s by Kh.S. Bagdasarov in the Institute of Crystallography named after A.V. Shubnikov of the Russian Academy of Sciences (Moscow) and is based on using thermal units made of Mo and W, Mo containers and reducing atmosphere [12,13]. YAP: Ho crystals were grown in high-purity Mo tubes in Ar/H₂ (10%) atmosphere, using YAP seeds oriented along the b-axis, and 2 mm/h lowering speed. Concentration of $\mathrm{Ho^{3+}}$ ions was 1.5 at.% in respect to $\mathrm{Y^{3+}}$. Interaction with the container metal leads to dissolution of some Mo in the melts, a part of which is absorbed by the crystal. Mo³⁺ centers were observed in EPR spectra of YAP crystals grown by the method of horizontal directional solidification in Mo containers [14]. The measured concentration of Mo³⁺ in YAG crystal grown by the Bridgman method, which has a close to YAP melting point is $8 \cdot 10^{-3}$ at.% [15]. The produced YAP: Ho crystals with length of 50-60 mm contain no twins or light-scattering inclusions, are colorless and are not colored under long-term daylight exposure. They were not subjected to any post-growth thermal treatment.

Measurements were made on a tunable EPR spectrometer [16] at liquid helium temperature in magnetic fields of up to 9kG. Several spectra were recorded while the sample was warmed up by a few degrees. A number of paramagnetic centers were found. The most intence signal that belonged to isolated Ho³⁺ ion, with a characteristic hyperfine (HF) structure, comprising 8 lines was observed in the frequency range of 150-230 GHz. configuration of Ho³⁺ is 4f¹⁰ ion, the ground state of the free ion is ${}^{5}I_{8}$ (L=6, S=2, J=8). In the local crystal field of C_s symmetry all electron multiplets are split into orbital singlets. The spectra we observe are related to resonance transitions between the ground and first excited singlets. Figure 1 presents the type of EPR spectra of Ho³⁺ ion recorded at frequency of 165 GHz in the orientation, when the magnetic field is in the plane (ab) and deviates from direction b by angle $\varphi = 37^{\circ}$.

Since the second excited level is located at the distance from the primary one with an energy interval of more than $30\,\mathrm{cm^{-1}}$, in the first approximation you may assume that holmium forms a two-level system. In this case non-Kramers $\mathrm{Ho^{3+}}$ ion has only one component of g-tensor not equal to zero ($g_{ZZ}=g$, directions of magnetic axes \mathbf{Z} of Ho1 and Ho2 centers were defined from angular dependences of the spectra). Angular dependences are described by the inverse cosine function. EPR signals are observed in the collinear mutual polarization of static and alternating magnetic fields ($\mathbf{B}_0 \parallel \mathbf{B}_1$). The experimental angular dependence of the spectra at rotation of the crystal in the (ab) plane is shown in Figure 2.

For clarity the figure presents the values of resonant magnetic fields of only low-field components of HF structure. In case of C_z symmetry, magnetic axes **Z** of Ho1 and Ho2 centers lie in the plane (ab), perpendicular to the normal

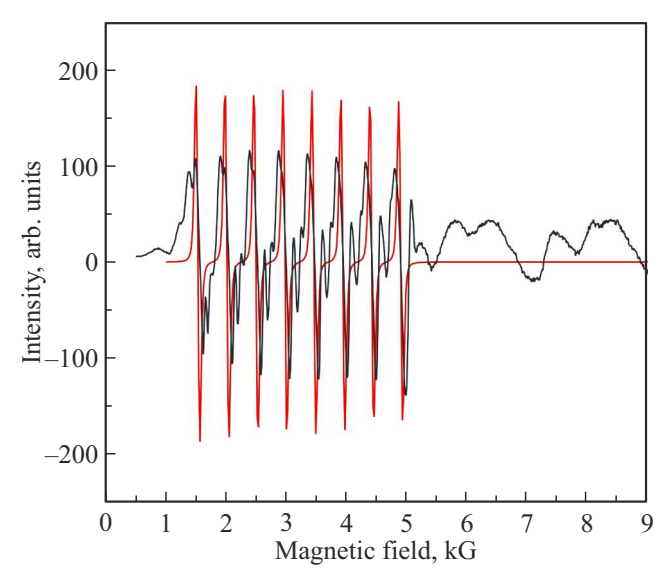


Figure 1. Measured (black line) and calculated (red line) EPR signals at a frequency of 165 GHz of a single Ho1 center; the magnetic field is directed at an angle of 37° to axis b in plane (ab). Additional lines in fields $B > 5 \, \mathrm{kG}$ correspond to resonance transitions in Ho2 centers.

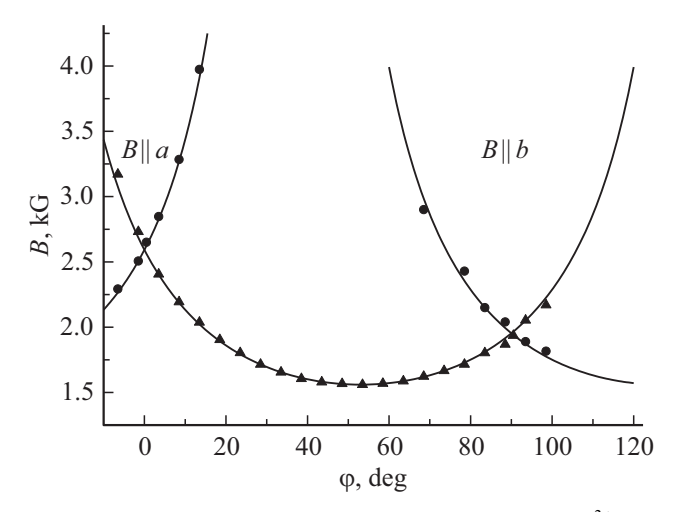


Figure 2. Angular dependence of EPR spectra of Ho^{3+} ions in YAlO₃ crystal. Rotation in plane (ab). Frequency 165 GHz. Symbols (triangles — Ho1 centers, circles — Ho2 centers) correspond to the measurement data, lines — to inverse cosine function.

line to the reflection plane. Direction of g-factor is deviated by 37° (Ho1) and -37° (Ho2) from axis b. For Ho1 centers the frequency-field dependence of EPR spectra measured in direction of axis \mathbf{Z} is compared to the results of calculations (see the next paragraph) in Figure 3.

Weaker satellite lines are superimposed onto eight HF structure lines of singlet-singlet transition (Figure 1) of the isolated center. Their origin is related to formation of antisite-defects near the isolated center. Due to high holmium concentration (1.5%), it was not possible to

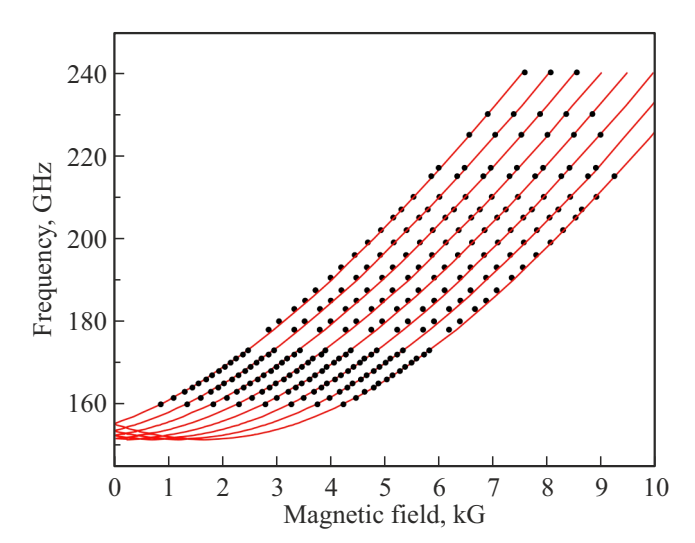


Figure 3. Measured (symbols) and calculated (solid lines) frequency-field dependences of EPR signals in single centers in magnetic fields oriented in direction of maximum *g*-factor.

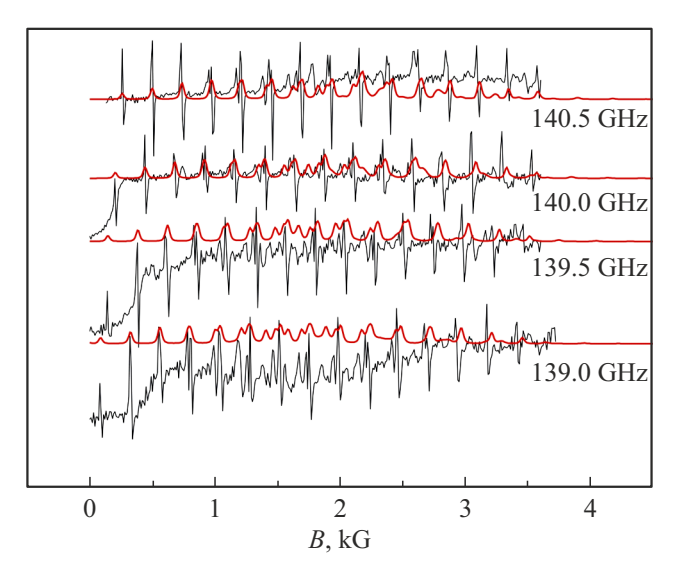


Figure 4. Measured (black lines) and calculated (red lines) absorption spectra of dimer formed by two closest magnetically equivalent Ho1 ions, in magnetic fields parallel to the direction of the maximum g-factor of the main doublet of Ho1 single centers.

separate the spectra from different centers. However, the presence of satellites next to the lines of the isolated center indicates that they have close values of g-factors, HF structure constants and splittings in the zero field. Note that imposition of additional lines onto the holmium spectrum deteriorated the accuracy of finding the center of the lines and led to higher error in the determination of spectral parameters.

A paired Ho³⁺-Ho³⁺ center was also found in the aluminate crystal. Examples of dimer spectra are shown in Figure 4.

Figure 5 shows frequency-field dependences of resonant transitions of dimer (low-frequency excitation branch)

measured in the same orientation as for the isolated In the zero magnetic field the electronic spectrum of dimer contains four lower states ($|1\rangle = (0, 0)$, both ions in the ground state; $|2\rangle = [(1,0) - (0,1)]/\sqrt{2}$ and $|3\rangle = [(1,0) + (0,1)]/\sqrt{2}$, when one of ions is excited, energy of states $|2\rangle$ and $|3\rangle$ differ due to the interaction between ions; $|4\rangle = (1, 1)$, both ions are excited). With account of spin moments of nuclei, the degeneracy factor of each state is 64. Thus, at frequencies below 300 GHz, it is possible to observe two branches of magnetic dipole parity allowed transitions $(|1\rangle \rightarrow |3\rangle$ and $|3\rangle \rightarrow |4\rangle$). In accordance with the measurement results, the low frequency branch of EPR spectra of dimers, which starts near frequency 132 GHz, corresponds to transitions $|3\rangle \rightarrow |4\rangle$, the second branch appears at frequency $\sim 170\,\text{GHz}$ and corresponds to transitions from the ground level $|1\rangle \rightarrow |3\rangle$. This is indicated by the growth of intensity of the low frequency branch lines at a minor (by several degrees) increase of temperature. The angular dependence of dimer spectra is identical to the dependence of the isolated spectra. For the low frequency branch at frequencies above 140 GHz 15 HF structure lines were observed. However, the intensity of the lines is not described by ratio 1:2:3:4:5:6:7:8:7:6:5:4:3:2:1, which is valid when only the diagonal component (AJ_ZI_Z) of the hyperfine interaction is taken into account, although the intensities from the outer to the center lines of the spectrum increase. The lines of the isolated center limited the area of observation of resonant transitions in the range of high-frequency dimer branch. As can be seen from Figure 3, the observation of such transitions in our

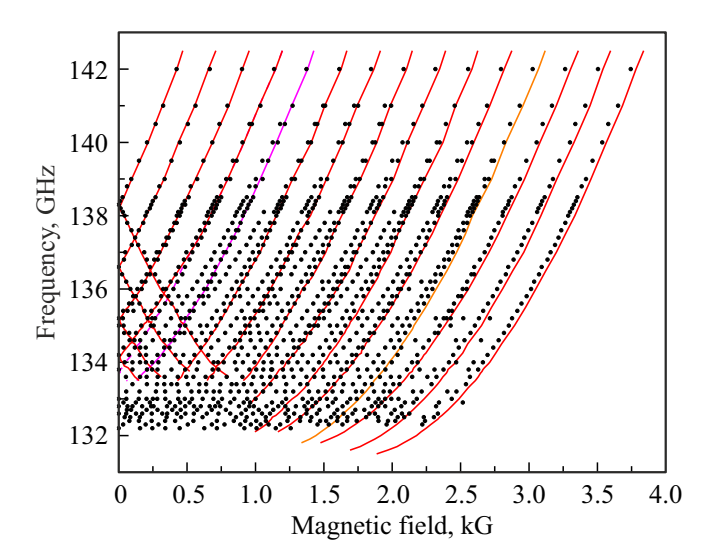


Figure 5. Measured (symbols) and calculated (solid lines) frequency-field dependences of the recorded EPR signals of paired centers of Ho³⁺ ions in the closest magnetically equivalent positions of Ho1 in the magnetic fields parallel to the corresponding magnetic axis **Z**. The dotted line in the frequency range of 134–138 GHz presents, as an example, additional signals that appear in weak magnetic fields.

spectrometer was only possible in the magnetic fields of up to $2\,\mathrm{kG}$. In the large magnetic fields the lines of isolated and paired centers were imposed. A frequency-field dependences were built for the low-frequency branch (Figure 5). The weak magnetic fields demonstrated splitting of 15 dimer lines into multiple components (note that the complete number of possible transitions in every branch is equal to $64 \cdot 64 = 4096$). In the frequency range $132-135\,\mathrm{GHz}$ it was not possible to follow their frequency-field dependence due to the overlap of the lines.

3. Calculations of spectra and discussion

A lattice cell of dielectric orthorhombic crystals YAlO₃ (the space group of symmetry Pbnm (D_{2h}^{16}), lattice distances $a=0.518\,\mathrm{nm},\ b=0.533\,\mathrm{nm},\ c=0.7375\,\mathrm{nm}$) contains four Y³+ ions in positions with local C_s symmetry with coordinates (in units of lattice constants a,b,c) $\mathbf{r}_{Y1}=(t,p,1/4),\ \mathbf{r}_{Y2}=-\mathbf{r}_{Y1},\ \mathbf{r}_{Y3}=(1/2-t,p+1/2,1/4),\ \mathbf{r}_{Y4}=-\mathbf{r}_{Y3},$ where t=-0.01192 and p=0.05305 [17,18]. Impurity holmium ions substitute for yttrium ions in the specified positions and form two types of magnetically inequivalent paramagnetic centers, Ho1 (in positions Y1 and Y2) and Ho2 (in positions Y3 and Y4).

Hamiltonian of Ho³⁺ ions used in modeling the results of EPR spectra measurements, determined in the full space of 1001 electron states of electronic configuration 4f¹⁰, has the form

$$H = H_{\rm FI} + H_{\rm CF} + H_{\rm Z}.\tag{1}$$

In operator (1) $H_{\rm FI}$ — parameterized standard Hamiltonian of free ion [19], $H_{\rm CF}$ — energy of interaction with the static crystal field, $H_{\rm Z}$ — energy of interaction with the external magnetic field ${\bf B}_0$. In accordance with the local C_s symmetry in the Cartesian coordinate system with axes x,y,z, directed along crystallographic axes b,c,a, accordingly, operator $H_{\rm CF}$ will takes the form

$$H_{\text{CF}} = B_2^0 O_2^0 + B_2^1 O_2^1 + B_2^2 O_2^2 + B_4^0 O_4^0 + B_4^1 O_4^1$$
$$+ B_4^2 O_4^2 + B_4^3 O_4^3 + B_4^4 O_4^4 + B_6^0 O_6^0 + B_6^1 O_6^1$$
$$+ B_6^2 O_6^2 + B_6^3 O_6^3 + B_6^4 O_6^4 + B_6^5 O_6^5 + B_6^6 O_6^6, \quad (2)$$

where O_q^p — linear combinations of spherical tensor operators summed over 4f electrons [20].

Calculations of the crystal field parameters B_q^p (CFP) are performed within the framework of the exchange charge model [21]. CFP of centers Ho1 and Ho2 are equal in absolute value but have opposite signs at p=1,3,5. Results of the calculations adjusted on the basis of comparison of calculated and measured resonant magnetic fields are given in Table 1.

The energies of Stark sublevels of the ground and first excited multiplets of holmium ions, calculated using the

Table 1. Crystal field parameters (cm⁻¹) for Ho1 and Tm1 centers in YAlO₃: Ho and YAlO₃: Tm crystals

q p	Ho1	Tm1
2 0	15.44	10.44
2 1	755.1	705.1
2 2	245.3	218.3
4 0	28.51	33.51
4 1	-1076.9	-956.9
4 2	-154.5	-154.5
4 3	-984.8	-924.8
4 4	-324.0	-289.0
6 0	59.13	59.13
6 1	19.7	19.7
6 2	178.9	177.9
6 3	159.4	159.4
6 4	-381.8	336.8
6 5	406.7	426.7
6 6	352.0	361.99

above CFP are compared to the results of optical spectroscopy [22] in Table 2 (own values and wave functions of the operator $H_0 = H_{\rm FI} + H_{\rm CF}$ were obtained by numerical diagonalization of the corresponding matrix constructed in the space of Slater determinants of the electron shell 4f¹⁰). Table 2 also shows the irreducible representations of C_s group, which describe the symmetry of the corresponding ion levels. Operators of components of electronic magnetic moment \mathbf{M} (projections on axis a,b,c) have matrix elements $\langle \Gamma 1i|M_a|\Gamma 2j\rangle$ and $\langle \Gamma 1i|M_b|\Gamma 2j\rangle$ different from zero. The calculated maximum g-factor of the ground electron quasi-doublet (effective spin S=1/2) with energies $E_1=0$ and $E_2=5.06\,\mathrm{cm}^{-1}$ is

$$g = 2[(M_{a,12})^2 + (M_{b,12})^2]^{1/2}/\mu_B$$
 (3)

(μ_B — Bohr magneton) is equal to 15.8 in the magnetic field directed in the plane ab at an angle $+39^{\circ}$ and -39° to b axis for Ho1 and Ho2 centers, accordingly.

The additional substantiation of the physical sense in the CFP set obtained in this paper and given in Table 1, apart from the quite precise description of magnetic characteristics and qualitative agreement of the calculated Stark structure of two lower multiplets of holmium ions with the data of optical spectroscopy [22], is the opportunity that opened to reproduce the magnetic characteristics of non-Kramers Tm3+ impurity ions (ground electronic configuration 4f¹²) in YAlO₃ crystal, measured in paper [11], using only comparatively small changes in CFP of Ho³⁺ ions (Table 1). In particular, we obtained splitting of the main quasi-doublet in the zero magnetic field $\Delta = 3 \, \text{cm}^{-1}$ $(2.97\,\mathrm{cm}^{-1})$, maximum g-factor 10.31 (\sim 10) and corresponding magnetic axis **Z** in the plane (ab) at angle 36.2° (35°) to b axis (the brackets contain the measurement data [11]).

Table 2. Energies E (cm⁻¹) and symmetry (Γ — irreducible representations) of sublevels of the ground (${}^{5}I_{8}$) and first excited (${}^{5}I_{7}$) multiplets of Ho³⁺ ion in the crystal field

№	Γ	Е	E [22]	№	Γ	Ε	E [22]
1	Г1	0	0	1	Г2	5199.1	5186
2	Γ2	5.06	6	2	Γ1	5199.4	5187
3	Γ2	31.35	37	3	Γ2	5236.5	5222
4	Γ1	74.30	48	4	Γ2	5238.2	5253
5	Γ1	120.2	58	5	Γ2	5261.7	5255
6	Γ2	130.9	71	6	Γ1	5263.2	5264
7	Γ1	206.3	100	7	Γ2	5297.3	5266
8	Γ2	224.1	126	8	Γ1	5303.1	5268
9	Γ2	284.5	137	9	Γ1	5336.3	5280
10	Γ1	299.8	193	10	Γ2	5338.8	5288
11	Γ1	323.4	211	11	Γ1	5351.9	5318
12	Γ2	325.1	222	12	Γ2	5357.4	5326
13	Γ1	442.4	289	13	Γ1	5363.9	5337
14	Γ2	444.5	327	14	Γ2	5374.9	5346
15	Γ2	482.6	425	15	Γ2	5378.0	5357
16	Γ1	487.6	474	_	_	_	_
17	Γ1	501.7	499	_	_	_	_

Holmium has the only stable isotope 165 Ho with nuclear spin I=7/2. The operator of magnetic hyperfine interaction has the form [6]

$$H_{HF} = A_{HF} \sum_{k} \left\{ \mathbf{I} \mathbf{I}_{k} + \frac{1}{2} \left[O_{2,k}^{0} (3s_{kz} I_{z} - s_{k} \mathbf{I}) \right] + 3O_{2,k}^{2} (s_{kx} I_{x} - s_{ky} I_{y}) + 3O_{2,k}^{-2} (s_{kx} I_{y} + s_{ky} I_{x}) + 6O_{2,k}^{1} (s_{kx} I_{z} + s_{kz} I_{x}) + 6O_{2,k}^{-1} (s_{kz} I_{y} + s_{ky} I_{z}) \right] \right\}, \quad (4)$$

where summation occurs in 4f electrons with orbital and spin moments \mathbf{l}_k and \mathbf{s}_k , $A_{\rm HF}=2\mu_B\gamma_{\rm Ho}\hbar\langle 1/r^3\rangle_{4f}$, $\gamma_{\rm Ho}/2\pi=8.98\,\mathrm{MHz/T}$ — gyromagnetic ratio of nucleus 165 Ho, $\langle r^3\rangle_{4f}=9.7\,\mathrm{a.u.}$ [6]. As it appears from the performed calculations, when considering the sub-THz EPR, the electric quadrupole hyperfine interaction in holmium ions may be neglected.

The procedure to calculate the envelope EPR signals included projecting the operators $H_{zx} = \mu_B \sum_k (\mathbf{l}_k + 2\mathbf{s}_k) \mathbf{B}_0$ and $H_{\rm HF}$ onto the space of electronic-nuclear eigenwave functions of operator H_0 , corresponding to multiplets 5I_J (J=4,5,6,7,8). The resulting matrices with size (2S+1)(2L+1)(2I+1) are diagonalized numerically for the fixed values and directions of the magnetic field \mathbf{B}_0 .

Distributions of resonance absorption intensity at frequency ω in the spectral lines corresponding to transitions between hyperfine sublevels j and k of the ground (Γ) and excited (Γ') singlets, accordingly, depending on the magnetic field at temperature T were calculated using the step of field change $\delta B_1 = 5 \cdot 10^{-4} \,\mathrm{T}$ in accordance with

formula

$$I(\Gamma \to \Gamma', B_0) = \sum_{j \in \Gamma} \sum_{k \in \Gamma'} \left| \langle k(\mathbf{B}_0) | M_B | j(\mathbf{B}_0) \rangle \right|^2$$

$$\times \exp(-E_i(\mathbf{B}_0)/k_BT)I_0[E_k(\mathbf{B}_0) - E_i(\mathbf{B}_0) - \hbar\omega], \quad (5)$$

where M_B — projection of the ion magnetic moment operator onto the magnetic field direction, k_B — Boltzmann constant, and $I_0(B_0)$ — Lorentz shape function of individual transitions with variable width.

Modeling of EPR spectra of dimers (distance between ions in dimer $R_{12} = 0.373 \,\mathrm{nm}$), containing the closest magnetically equivalent Ho1 ions (in positions \mathbf{r}_{Y1} and \mathbf{r}_{Y2}) or Ho2 ions (in positions \mathbf{r}_{Y3} and \mathbf{r}_{Y4}), was carried out using Hamilton operator

$$H_{\text{dim}} = H(1) + H(2) + H_{\text{dip}}(1, 2) + H_{\text{ex}}(1, 2),$$
 (6)

where energies of magnetic interactions (dipole-dipole H_{dip} and isotropic antiferromagnetic exchange H_{ex}) were added to the sum of energies of isolated ions (see (1)). Operator of exchange interaction $H_{\rm ex}(1,2) = J_{\rm ex} \mathbf{S}_1 \cdot \mathbf{S}_2$ (where \mathbf{S}_i operator of full spin moment of ith ion) contains the only variable parameter of the model, the exchange integral $J_{\rm ex}$, the value of which $(J_{\rm ex}=0.17\,{\rm cm}^{-1})$ was determined from the comparison of the calculated envelope absorption spectra (Figure 4) and frequency-field dependences of EPR signals (see Figure 5) with the measurement data. The calculations were carried out in the space of the dimer states determined by the Kronecker product of subspaces of electronic-nuclear wave functions of the main non-Kramers doublets of two holmium ions, using the intensity distribution, similar to (5), where the operator of magnetic moment of one ion is substituted with a sum of magnetic moments of two ions) and frequency-field dependences of EPR signals with measurement data (Figure 5). The dimer axis only slightly deviates from c axis and, since the magnetic moments of isolated ions lie in plane ab, antiferromagnetic exchange interaction strengthens the magnetic dipole interaction between ions. Within the Russell-Saunders coupling scheme the energy of magnetic dipole interaction is obtained as $H_{\text{dip}} = D(S_{1a}S_{2a} + S_{1b}S_{2b})$, where $D = \mu_B^2 (1 - 1/g_J)^{-2}/R_{12}^3$ and $g_J = 5/4$ — Lande factor of multiplet ⁵I₈. Therefore, in the considered dimers of holmium ions the exchange and magnetic dipole $(D = 0.21 \,\mathrm{cm}^{-1})$ interactions have comparable values. Let us note that the magnetic properties of the dimers of ytterbium impurity ions in the YAIO₃ crystal with similar structure, in which the dominant role belongs to exchange antiferromagnetic interaction, were studied in [23].

4. Conclusion

Despite the fact that spectral and magnetic properties of diluted and concentrated rare-earth aluminates have been studied for decades, and some YAlO₃ crystals activated by Er³⁺, Tm³⁺, Ho³⁺ ions are already used in lasers to obtain

the stimulated radiation in various frequency ranges [24], the parameters of the crystal field (CFP), acting at rareearth ions in positions with local C_s symmetry, remain unknown due to the lack of information on the structure of the operator's eigenfunctions to build the operator $H_{\rm CF}$ — wave functions of Stark sublevels of electronic multiplets. The only set of 15 CFP that we know is given in Ref. [25] for Tm³⁺ ions is unreliable, since the energy of the first excited state (31 cm⁻¹) obtained using these parameters is by an order of magnitude higher than the experimental value (3 cm⁻¹ [11]).

In this paper we have measured the low-temperature spectra of sub-THz EPR Van Vleck paramagnetic $YAlO_3: Ho^{3+}$ (1.5%). Two types of paramagnetic centers were found, formed by isolated Ho³⁺ ions in magnetically inequivalent positions of Y³⁺ ions, and dimers containing the closest magnetically equivalent Ho³⁺ ions. The spectra of isolated centers have the resolved hyperfine structure. The observed spectral lines correspond to the resonant transitions between the hyperfine sublevels of the ground and first excited singlets in the ground multiplet ⁵I₈. The value of Stark splitting between these singlets is measured. Directions of the maximum g-factor of magnetically inequivalent centers lie in plane (ab) and are turned away from the crystallographic direction b by $+37^{\circ}$ and -37° . Based on the analysis of the spectra and calculations within the exchange charge model, CFP were determined the use of which made it possible to reproduce the measurement results.

Dimer spectra comply with the resonant transitions between the electronic-nuclear sublevels of four electronic levels of two non-Kramers quasi-doublets. According to the rules of selection by parity, transitions were observed from the ground to the second excited level and from the second excited to the third excited level. Two frequencyfield dependences of transitions were constructed for the corresponding branches of the excitation spectrum. The high-frequency branch of the dimer spectrum was imposed on the excitation spectrum of isolated centers and was recorded in the limited range of magnetic fields. low-frequency branch of the spectrum has a complicated structure that contains multiple intense and weak lines. The calculation of the dimer spectrum, apart from energies of isolated ions, took into account the magnetic dipoledipole and isotropic antiferromagnetic exchange interaction. The obtained value of the exchange interactions in the dimers may be used to built the theory of antiferromagnetic electron-nuclear ordering found at $T_N = 0.16 \,\mathrm{K}$ in the concentrated compound HoAlO₃ [26].

Acknowledgments

The authors would like to thank V.A. Shustov for orientation of the crystal on the X-ray diffractometer.

Funding

The study in the Zavoisky Physical-Technical Institute was performed under the state assignment of the Federal Research Center Kazan Scientific Center of the Russian Academy of Sciences. The work of BZM was supported by the subsidy provided to the Kazan Federal University to perform the state assignment in the field of science (project No. FZSM-2024-0010), and of AGP by the State Science Committee of the Republic of Armenia within project No. 1-6/23-I/IPR.

Conflict of interest

The authors declare that they have no conflict of interest.

References

- [1] A.A. Kaminskii. Crystalline Lasers: Physical Processes and Operating Schemes, CRC Press (1996). Section 1.4.5.
- [2] Kh.S. Bagdasarov, A.A. Kaminsky. Pisma in ZhETF 9, 501 (1969). (in Russian).
- [3] J. Sulk, M. Nemec, M. Jelínek, H. Jelínkova, V. Kubecek, K. Nejezchleb, J. Polak. Proc. SPIE 11980, 119800D (2022).
- [4] M. Malinowski, M. Kaczkan, A. Wnuk, M. Szuflinska. J. Lumin. 106, 269 (2004).
- [5] E. Galluci, C. Dujardin, M. Boudeulle, C. Pedrini, A.G. Petrosyan, T. Hansen. In: Proceedings of International Conference on Inorganic Scintillators and Their Applications (SCINT'99). Moscow (2000). P. 506–510.
- [6] D.S. Pytalev, E.P. Chukalina, M.N. Popova, G.S. Shakurov, B.Z. Malkin, S.L. Korableva. Phys. Rev. B 86, 115124 (2012).
- [7] A.A. Konovalov, D.A. Lis, B.Z. Malkin, S.I. Nikitin, K.A. Subbotin, V.F. Tarasov, E.N. Vorobieva, E.V. Zharikov, D.G. Zverev. Appl. Magn. Reson. 28, 267 (2005).
- [8] G.S. Shakurov, E.P. Chukalina, M.N. Popova, B.Z. Malkin, A.M. Tkachuk. Phys. Chem. Chem. Phys. 16, 24727 (2014).
- [9] G.R. Asatryan, G.S. Shakurov, A.G. Petrosyan, D.D. Kramuschenko, K.L. Ovanesyan. FTT 64, 6, 697 (2022). (in Russian).
- [10] G.R. Asatryan, G.S. Shakurov, N.M. Lyadov, K.L. Hovhannesyan, A.G. Petrosyan. Opt. Memory Neural Networks 32, 3, S356 (2023).
- [11] G.R. Asatryan, A.P. Skvortsov, G.S. Shakurov. FTT 55, 958 (2013). (in Russian).
- [12] A.A. Chernov, E.J. Givargizov, K.S. Bagdasarov, V.A. Kuznetsov, L.N. Demianets, A.N. Lobachev. Modern Crystallography III: Crystal Growth (Springer Series in Solid-State Sciences, vol. 36). Springer, Berlin (1984).
- [13] A.G. Petrosyan. J. Cryst. Growth 139, 372 (1994).
- [14] G.R. Asatryan, J. Rosa. FTT 44, 5, 830 (2002). (in Russian).
- [15] E.A. Markosyan, A.G. Petrosyan, E.G. Sharoyan. FTT 15, 2504 (1973). (in Russian).
- [16] V.F. Tarasov, G.S. Shakurov. Appl. Magn. Reson. 2, 3, 571 (1991).
- [17] R. Diehl, G. Brandt. Mat. Res. Bull. 10, 85 (1975).
- [18] N.L. Ross, J. Zhao, R.J. Angel. J. Solid State Chem. 177, 1276 (2004).
- [19] W.T. Carnall, G.L. Goodman, K. Rajnak, R.S. Rana. J. Chem. Phys. 90, 3443 (1989).

- [20] V.V. Klekovkina, A.R. Zakirov, B.Z. Malkin, L.A. Kasatkina. J. Phys. Confer. Ser. 324, 012036 (2011).
- [21] B.Z. Malkin. In: Spectroscopy of solids containing rare earth ions / Eds. A.A. Kaplyanskii, R.M. Macfarlane. North-Holland, Amsterdam (1987). Ch. 2. P. 13.
- [22] B.-Q. Yao, X.-M. Duan, L.-L. Zheng, Y.-L. Ju, Y. Wang, G.-J. Zhao, Q. Dong. Opt. Express 16, 19, 14668 (2008).
- [23] S.E. Nikitin, Tao Xie, A. Podlesnyak, I.A. Zaliznyak. Phys. Rev. B 101, 245150 (2020).
- [24] F. Cassouret, A. Nady, P. Loiko, S. Normani, A. Braud, W. Chen, V. Petrov, D. Sun, P. Zhang, B. Viana, A. Hideur, P. Camy. Opt. Lett. 49, 2970 (2024).
- [25] J.M. O'Hare, V.L. Donlan. Phys. Rev. B 14, 3732 (1976).
- [26] J. Hammann, M. Ocio. J. Magn. Magn. Mater. **15–18**, 39 (1980).

Translated by M.Verenikina